JOURNAL OF MATERIALS SCIENCE **33** (1998) 4911–4915

The chemical and morphological properties of boron–carbon alloys grown by plasma-enhanced chemical vapour deposition

D. ZHANG, D. N. MCILROY*
Department of Physics, Engineering and Physics Building, University of Idaho, Moscow, ID 83844-0903, USA

W. L. O'BRIEN
Synchrotron Radiation Center, University of Wisconsin-Madison, 3731 Schneider Dr., Stoughton, WI 53589-3097, USA

G. DE STASIO
Institut de Physique Appliquée, Ecole Polytechnique Fédérale, CH-1015 Lausanne, Switzerland and Istituto di Struttura della Materia del CNR, Via Fosso del Cavaliere, I-00137, Roma, Italy

The stoichiometry and morphology of boron–carbon alloy thin films grown by plasma-enhanced chemical vapour deposition can be significantly modified by varying the deposition rate. Films grown at a rate of 5.5 nm min^{-1} are characterized by an amorphous-like matrix with carbon-rich and dome-like inclusions. Films grown at a deposition rate of 33 nm min^{-1} are found to be much more homogeneous and free of carbon-rich and dome-like inclusions. An excitation at 191.7 eV in the B 1s absorption spectrum has been associated with amorphous growth. The relative intensities of the π^* and σ^* excitations across the C 1s absorption edge of these boron-carbon alloys indicate that carbon bonding is predominantly through sp^3 hybridization, while boron bonding is a mix of sp^2 and sp^3 hybridization.

1. Introduction

In recent years it has been demonstrated that high temperature semiconductor devices can be constructed from boron–carbon alloys (B_5C) grown by plasma-enhanced chemical vapour deposition (PECVD) [1–6]. These boron–carbon (BC) alloys are refractory materials with bandgaps of the order of 0.7 eV [1, 7]. The undoped BC alloys are intrinsically doped *p*-type semiconductors [1–3], while nickel-doped BC alloys have been found to be *n*-type [4–6]. Consequently, it has been possible to construct simple homojunction diodes with doped and undoped thin films of these BC alloys which can operate effectively at temperatures in excess of 300 °C [5, 6].

The composition of these BC alloys consists of nanoparticles embedded in an amorphous matrix [8, 9]. This is in contrast to single-crystal boron carbide which has a rhombohedral structure consisting of $B_{11}C$ icosahedra interconnected with CBC chains [10–13]. In addition to their structural differences, these two types of boron–carbon materials have quite different electrical properties. The undoped BC alloys typically have conductivities of 10^{-10} to 10^{-12} Ω cm^{-1} [1], as compared to single crystal boron carbide which has a conductivity of 1 Ω cm^{-1} [14]. This is consistent with the low carrier concentration of these BC alloys [1]. It is the high resistivity and low carrier concentrations which make these BC alloys useful for high temperature semiconductor applications, as opposed to thermal power applications which is the typically proposed application for single-crystal boron carbide [15–17].

Currently, very little is known about the chemical composition of these BC alloys beyond preliminary i.r. absorption [5, 9] and Auger measurements [1]. The i.r. measurements revealed the existence of C—H and B—H vibrational modes which agreed with similar measurements of BC alloys grown by chemical vapour deposition using different precursors from those used in this study [18–19]. To date, these are the only measurements of the chemical composition of these alloys that the authors are aware of.

In order to further our understanding of the composition of these BC alloys grown by PECVD, we have performed what we believe to be the first near edge X-ray absorption spectroscopy (NEXAFS) measurements on these alloys using synchrotron radiation in conjunction with an imaging photoelectron spectromicroscope. By coupling these two techniques we can

* Author to whom correspondence should be addressed.

simultaneously image and acquire elemental specific information about the chemical composition of distinct regions of the BC alloys. By using total electron yield to measure NEXAFS we are able to probe 5–10 nm below the sample surface [20]. Consequently, we are not restricted to probing only the surface composition of these BC alloys. In addition to obtaining important spectroscopic information, we will demonstrate the strength of synchrotron-coupled photoelectron spectral microscopy for materials characterization and evaluation.

2. Experimental procedure

The samples were grown using the single source compound orthocarborane (*closo*-1,2-dicarbadodecaborane ($C_2B_{10}H_{12}$)). Orthocarborane is a crystalline powder which is easily sublimed. In the present case, the compound was delivered to the deposition chamber by heating the source bottle to 80 °C while simultaneously passing Ar through the source bottle. The gas flow through the source bottle was 10 s.c.c.m. with an additional Ar flow of 10 s.c.c.m. into the chamber. The pumping was throttled down to give a total chamber pressure of 39.9 Pa. The films were deposited on Si(1 1 0) substrates which were cleaned in a 5% hydrofluoric acid/deionized water solution prior to insertion into the plasma chamber. The substrates were subsequently sputtered in Ar prior to deposition. The Si substrates were maintained at 300 °C during deposition. The plasma chamber is a parallel plate design with a base pressure of 1.33×10^{-5} Pa. The samples were located on the grounded anode. The plasma power was 50 W at a frequency of 13.56 MHz. By varying the position of the gas delivery nozzle relative to the substrate the deposition rate was varied from 5.5 nm min^{-1} (Sample A) to 33 nm min^{-1} (Sample B).

The imaging and the NEXAFS spectra were acquired using the imaging photoelectron spectromicroscope MEPHISTO [21] which was attached to the 10-m TGM beamline at the Synchrotron Radiation Center in Stoughton, WI. Briefly, monochromatic soft X-rays are incident on the sample at 60° off the surface normal with the photoelectrons collected over a 2π sterad spherical angle. The fundamental mode of operation of the microscope is photoelectron emission by X-ray excitation. Consequently, elemental imaging and NEXAFS spectra are acquired by setting the monochromator at an absorption edge, for instance the carbon edge at 293 eV, and collecting the photoelectrons emitted. Specific details of the microscope are discussed in greater detail elsewhere [21]. The microscope base pressure was 2.67×10^{-8} Pa. The C 1s NEXAFS spectra were normalized to the photon flux. This normalization procedure eliminates spurious structure from being introduced into the C 1s spectra by carbon contamination on the beamline optics. The surfaces of the samples were found to be relatively free of oxygen upon examination of the intensity of the O 1s absorption edge.

3. Results and discussion

In Fig. 1 we present the microscope images of Sample A and Sample B. The images of Sample A were acquired at the B 1s (Fig. 1a) and the C 1s (Fig. 1b) absorption edges, respectively. The images indicate that the surface of Sample A is essentially flat with the exception of dome structures ranging in diameter from approximately 7 to 26 μm. One limitation of this microscopic technique is its inability to distinguish between concave and convex structures. In the case of Sample A, we have been able to determine that the circular blemishes, henceforth referred to as domes, protrude from the surface based on the following argument. The shadowing effect observed for the dome labelled 1 in Fig. 1a and b is independent of whether the image was acquired across the boron edge or the carbon edge. This rules out explanations based on lateral variations of the chemical composition of the domes. Instead, we can resolve this issue using simple geometric arguments. Because the X-rays impinge of the sample from the left side at an angle of 60°, large blemishes protruding from the surface will effectively shadow their right side from the X-rays, regardless of the X-ray energy. This is consistent with the observed shadowing of the blemish labeled 1 in Fig. 1a and b. In fact, shadowing is observed for the majority of blemishes (domes) in Fig. 1a and b.

In addition to the domes, there is a region (labelled 2 in Fig. 1a) which appears significantly darker than the rest of the image acquired at the boron absorption edge. In contrast, this same region is brighter than the majority of the image in Fig. 1b which was acquired at the carbon absorption edge. Because the brightness of a given region is directly proportional to the absorption, which in turn is proportional to the elemental concentration, we can conclude that region 2 has a higher carbon concentration relative to the majority of the BC film, thereby explaining its dark appearance at the boron edge and its bright appearance at the carbon edge.

In stark contrast to the images of Sample A are those of Sample B (Fig. 1c and d) which was grown at a higher deposition rate (33 nm min^{-1}). We no longer observe the formation of large domes or carbon-rich regions. In fact, the film is extremely uniform with the exception of small blemishes, approximately 1 μm in diameter, which may be surface contaminants or pin holes. The images of Sample B were acquired on the border between two regions of differing thickness. In the image of Sample B acquired at the carbon edge (Fig. 1d) there is a very sharp boundary between a darker region (1′) and a lighter region (2′) which indicates that region 2′ has a slightly higher carbon concentration. In contrast, this boundary is invisible in the image of Sample B (Fig. 1c) acquired at the boron absorption edge. This suggests that there may be different termination surfaces depending on the film thickness and that the growth mode under these conditions may be layer by layer. These issues will need to be examined in greater detail before a definitive conclusion can be reached.

Details about the chemical composition of these alloys can be obtained by examining their corresponding NEXAFS spectra. In particular, we have been able to take advantage of the imaging capabilities of

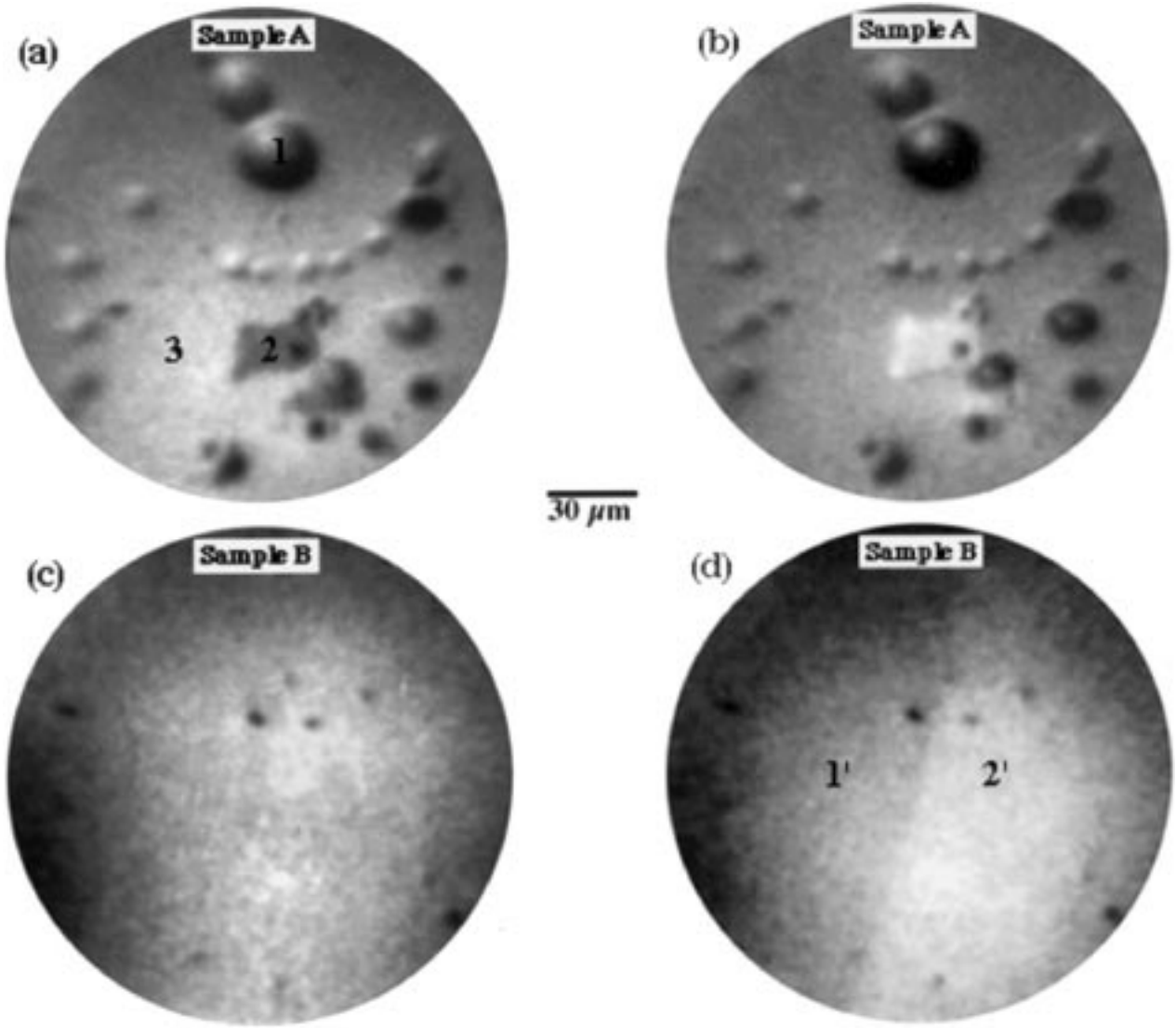

Figure 1 Photoelectron emission microscope (MEPHISTO) images of boron–carbon alloys (a) of Sample A acquired at the B 1s absorption edge at a photon energy of 192 eV; (b) Sample A at the C 1s absorption edge at a photon energy of 293 eV; (c) Sample B at the B 1s absorption edge at a photon energy of 192 eV; and (d) Sample B at the C absorption edge at a photon energy of 293 eV.

MEPHISTO to analyse the chemical composition of specific regions of the samples. For Sample A we have examined the chemical composition of regions 1–3 in Fig. 1a. The NEXAFS spectra are displayed in Fig. 2. The B 1s absorption edge is characterized by the onset of the antibonding π^* state at 190 eV and the σ^* states from 196 to 208 eV. The π^* and σ^* assignments are based on comparisons to single crystal boron carbide [23] and hexagonal boron nitride [24, 25]. The spectra of all three regions are essentially the same except for region 1 (dome) where we observe an extra feature labelled A in Fig. 2a. In addition, the π^* state of region 1 is sharper and narrower than the corresponding feature of the other two regions which have a pronounced shoulder at a photon energy at 192.6 eV.

These differences between region 1 and regions 2 and 3 are also manifested in the C 1s spectra. Again, spectral assignments are based on comparisons to single crystal boron carbide [23]. The σ^* states at 287.9 and 291 eV are much narrower than the corresponding features in the spectra of regions 2 and 3. Note that the intensity of the C 1s signal of region 2 is twice as larger as those of the other two regions. This supports our interpretation that region 2 is carbon-rich relative to the other regions of Sample A. Similar carbon-rich, or graphite-like, regions on the surfaces of hot pressed single crystals of boron carbide have been observed with Auger electron spectroscopy [22].

The relative intensities of the π^* states of the C 1s spectra relative to the σ^* states suggests that the carbon bonding within these boron–carbon alloys is a combination of sp^2 and sp^3 bonding, although we cannot rule out sp bonding. Based on the relative intensity of the C 1s π^* and σ^* states, we conclude that the carbon bonding is primarily sp^3 in character. In amorphous carbon it has been shown that film hardness increases with increased sp^3 bonding [26]. This is consistent with the relatively hard nature of these BC alloys.

The NEXAFS spectra of Sample B in Fig. 3 are dramatically different from those of Sample A. Upon comparing the B 1s spectra of Sample B in Fig. 3a with Fig. 2a, we see that what was a sharp feature at 191.8 eV in the spectra of Sample A is now a shoulder in the spectra of Sample B and what was a shoulder at 192.6 eV in the spectra of Sample A is now a sharp spectral feature (labelled B in Fig. 3a). Temperature

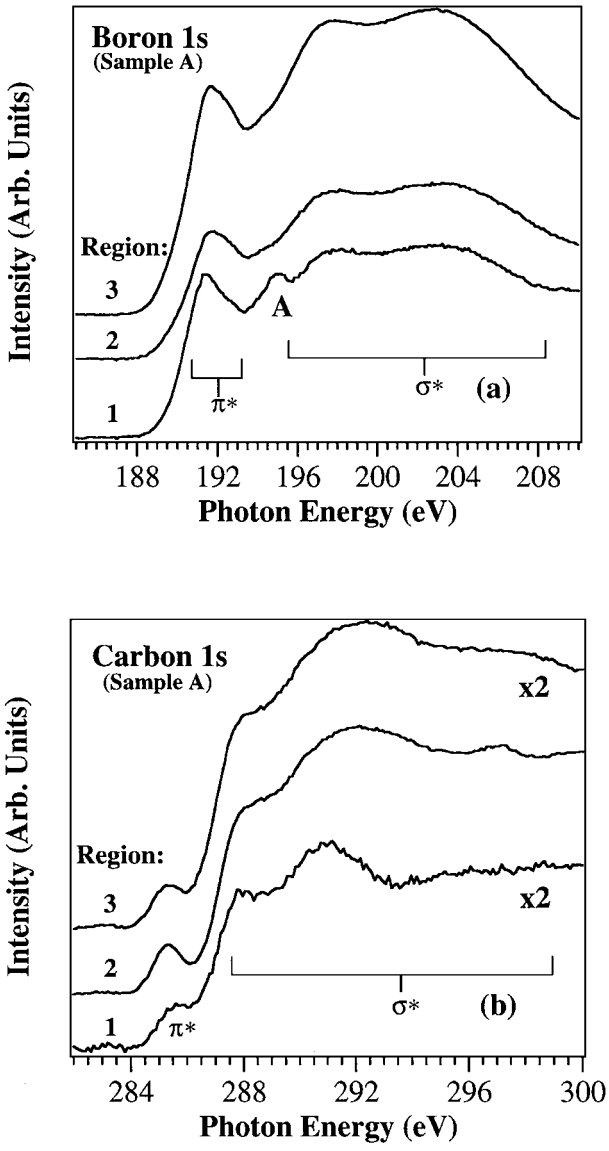

Figure 2 The NEXAFS spectra of regions 1, 2 and 3 of Sample A across (a) the B 1s absorption edge and (b) the C 1s absorption edge.

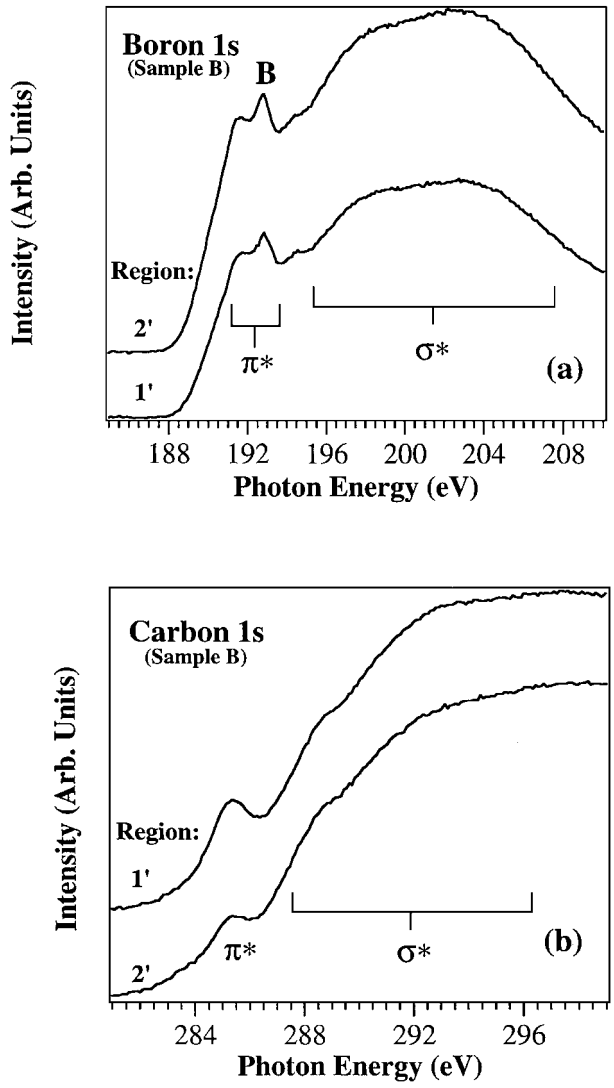

Figure 3 The NEXAFS spectra of regions 1 and 2 of Sample B across (a) the B 1s absorption edge and (b) the C 1s absorption edge.

dependent NEXAFS studies of single crystal boron carbide suggest that feature B is indicative of a phase or stoichiometry akin to boron powder [23]. Also, the σ^* states of Sample B are not as well resolved as they are in Fig. 2a of Sample A.

The C 1s NEXAFS spectra are also quite different between Sample A and Sample B and can provide information about carbon bonding within these BC alloys. The relative intensity of the C π^* state to the σ^* states gives a qualitative measure of ratio of sp/sp^2 hybridization to sp^3 hybridization. The intensity of the π^* state of Sample B, relative to the σ^* states, is substantially larger than in Sample A, as well as broader. Based on these comparisons we propose that a larger portion of bonding in Sample B is through sp and sp^2 hybridization, as compared to Sample A. In addition, the σ^* states of Sample B are poorly resolved and are more or less structureless.

Based on the high deposition rate (33 nm min^{-1}) and substrate temperature (300 °C) at which Sample B was grown, we suggest that the sharp feature at 192.8 eV in the B 1s absorption spectra and the broadening of the features in the C 1s absorption spectra are the signatures of an extremely homogeneous amorphous BC alloy. Consequently, we conclude that Sample A has greater short-range order relative to Sample B. This is consistent with atomic force microscopy measurements which identified the formation of BC nanocrystals on the order of 60–100 nm within an amorphous matrix [8]. The sharpness of the B 1s π^* state and the σ^* states in the C 1s absorption spectrum of the dome (region 1) in Sample A suggests that these structures possess a higher degree of homogeneity than the other regions of this BC film. Furthermore, we suggest that the domes form as a consequence of the slower deposition rate (5.5 nm min^{-1}) used to grow Sample A. This in turn increases the surface diffusion length and thereby allows the domes to form. This issue will need to be explored in further detail in order to understand the interplay between surface diffusion and the formation of domes.

4. Conclusions

We have examined the effects of the deposition rate of the PECVD process on the topography and chemical

composition of boron–carbon alloys using imaging photoelectron spectromicroscopy. We have found that a sample grown at a deposition rate of 33 nm min^{-1} is smoother and more homogenous than a sample grown at 5.5 nm min^{-1}. The relative intensity of the π^* and σ^* excitations in the C 1s absorption spectra of both samples indicates that carbon bonding is predominantly through sp^3 hybridization, while the boron atoms bond in a mixed configuration of sp^2 and sp^3 hybridization. The topography of the sample grown at 5.5 nm min^{-1} consists of carbon-rich regions and domed structures embedded in a smooth homogeneous matrix. The sharpness of the features in the NEXAFS spectrum of the domes, relative to the other regions of this sample, as well as the sample grown at a rate of 33 nm min^{-1}, suggests that the structure of these domes is more ordered than the other regions of this sample, or the sample grown at 33 nm min^{-1}. This is also supported by the absence of a pronounced peak at 191.7 eV in the B 1s absorption spectrum which we have identified with amorphous composition. These studies clearly demonstrate the need to further examine the growth kinetics of these boron–carbon alloys in order to determine the dependence of their electronic properties on their chemical composition with the goal of optimizing their high temperature device characteristics.

Acknowledgements

D.N.M. would like to acknowledge the support of the NSF-Idaho EPSCoR project under NSF Cooperative Agreement number EPS-9350539, a seed grant from the University of Idaho Research Council (KDY817), and the Petroleum Research Foundation (PRF# 32584-G5). This work was conducted at the Synchrotron Radiation Center, University of Wisconsin-Madison, which is supported by NSF under Award No. DMR-95-31009. The authors would like to acknowledge Ben Gilbert, Jose Redondo and John Failla for their assistance on this project.

References

1. S. LEE, J. MAZUROWSKI, G. RAMSEYER and P. A. DOWBEN, *J. Appl. Phys.* **72** (1992) 4925.
2. S. LEE and P. A. DOWBEN, *Appl. Phys.* **A 58** (1994) 223.
3. S.-D. HWANG, D. BYUN, N. J. IANNO, P. A. DOWBEN and H. R. KIM, *Appl. Phys. Lett.* **68** (1996) 1495.
4. S.-D. HWANG, N. B. REMMES, P. A. DOWBEN and D. N. MCILROY, *J. Vac. Sci. Technol.* **B 14** (1996) 2957.
5. S.-D. HWANG, KEN YANG, P. A. DOWBEN, AHMAD A. AHMAD, N. J. IANNO, J. Z. LI, J. Y. LIN, H. X. JIANG and D. N. MCILROY, *Appl. Phys. Lett.* **70** (1997) 1028.
6. D. N. MCILROY, S.-D. HWANG, KEN YANG, N. REMMES, P. A. DOWBEN, AHMAD A. AHMAD, N. J. IANNO, J. Z. LI, J. Y. LIN and H. X. JIANG, *Appl. Phys.* **A69** (1998) 335.
7. AHMAD A. AHMAD, N. J. IANNO, P. G. SNYDER, D. WELIPITIYA, D. DYUN and P. A. DOWBEN, *J. Appl. Phys.* **79** (1996) 1.
8. DONGJIN BYUN, B. R. SPADY, N. J. IANNO and P. A. DOWBEN, *Nanostructured Materials* **5** (1995) 465.
9. D. N. MCILROY *et al.*, in preparation.
10. D. R. TALLANT, T. L. ASELAGE and D. EMIN, "Boron-rich solids," edited by D. Emin, T. L. Aselage, A. C. Switendick, B. Morosin, and C. L. Beckel, AIP Cof. Proc. 231 (AIP, New York, 1991) p. 177.
11. U. KUHLMANN and H. WERHEIT, *Phys. Status Solidi B* **175** (1993) 85.
12. J. CONARD, M. BOUCHACOURT, F. THEVENOT and G. HERMANN, *J. Less-Common Metals* **117** (1986) 51.
13. E. L. VENTURINI, L. J. AZEVEDO, D. EMIN and C. WOOD, in "Boron-rich solids," edited by D. Emin, T. L. Aselage, C. L. Beckel, I. A. Howard, and C. Wood, AIP Conf. Proc. 140 (AIP, New York, 1986) p. 292.
14. CHARLES WOOD, in "Boron-rich solids," edited by D. Emin, T. L. Aselage, C. L. Beckel, I. A. Howard, and C. Wood, AIP Conf. Proc. 140 (AIP, New York, 1986) p. 206.
15. HELMUT WERHEIT, *Mater. Sci. Eng.* **B 29** (1995) 228.
16. H. WERHEIT, U. KUHLMANN, G. KRACH, I. HIGASHI, T. LUNDSTRÖM and Y. YU, *J. Alloys Comp.* **202** (1993) 269.
17. U. KUHLMANN, H. WERHEIT, J. PELLOTH, W. KEUNE and T. LUNDSTRÖM, *Phys. Status Solidi. (b)* **187** (1995) 43.
18. K. SHIRAI, S. EMURA, S. GONDA and Y. KUMASHIRO, *J. Appl. Phys.* **78** (1995) 3392.
19. J. I. OÑATE, A. GARCIA, V. BELLIDO and J. L. VIVIENTE, *Surf. Coat. Technol.* **49** (1991) 548.
20. D. J. G. SUTHERLAND, H. AKATSU, M. COPEL, F. J. HIMPSEL, T. A. CALLCOT, J. A. CARLISLE, D. L. EDERER, J. J. JIA, I. JIMENEZ, R. PERERA, D. K. SHUH, L. J. TERMINELLO and W. M. TONG, *J. Appl. Phys.* **78** (1995) 6761.
21. GELSOMINA DE STASIO, M. CAPOZI, G. F. LORUSSO, P. A. BAUDAT, T. C. DROUBAY, P. PERFETTI, G. MARGARITONDO and B. P. TONNER, *Rev. Sci. Instrum.* **69** (1998) 2062.
22. H. H. MADDEN, G. C. NELSON and W. O. WALLACE, in "Boron-rich solids," edited by D. Emin, T. L. Aselage, C. L. Beckel, I. A. Howard, and C. Wood, AIP Conf. Proc. 140 (AIP, New York, 1986) p. 121.
23. I. JIMÉNEZ, D. G. J. SUTHERLAND, A. VAN BUUREN, J. A. CARLISLE, L. J. TERMINELLO and F. J. HIMPSEL, unpublished.
24. I. JIMÉNEZ, A. JANKOWSKI, L. J. TERMINELLO, J. A. CARLISLE, D. G. J. SUTHERLAND, G. L. DOLL, J. V. MANTESE, W. M. TONG, D. K. SHUH and F. J. HIMPSEL, *Appl. Phys. Lett.* **68** (1996) 2816.
25. I. JIMÉNEZ, A. JANKOWSKI, L. J. TERMINELLO, D. G. J. SUTHERLAND, J. A. CARLISLE, G. L. DOLL, W. M. TONG, D. K. SHUH and F. J. HIMPSEL, *Phys. Rev. B* **55** (1997) 1225.
26. J. DÍAZ, G. PAOLICELLI, S. FERRER and F. COMIN, *Phys. Rev. B* **54** (1996) 8064.

Received 29 January
and accepted 2 July 1998